Technical Report No. 4
Contract 00014-84-K-0472; NR 650-025

SPRAY DEPOSITION : A FUNDAMENTAL STUDY OF DROPLET IMPINGEMENT, SPREADING AND CONSOLIDATION

D. Apelian, A. Lawley, G. Gillen and P. Mathur
Department of Materials Engineering
Drexel University
Philadelphia, PA 19104

December 1988

Prepared for
OFFICE OF NAVAL RESEARCH
800 N. Quincy Street
Arlington, VA 22217

INTRODUCTION

Spray deposition via the Osprey™ process is rapidly emerging as an attractive technology to produce net or near-net-shaped components of a variety of alloys [1-3]. The process is schematically shown in Fig. 1. The alloy charge is melted under an inert gas cover in a crucible placed on top of the spray chamber. At the appropriate superheat temperature, the molten metal is allowed to exit through a refractory nozzle at the base of the crucible into the atomizing zone. The stream of molten metal is gas atomized. Subsequently, the liquid droplets accelerate and cool/solidify under the influence of the atomizing gas, and consolidate on the substrate to form a homogeneous deposit. Spray deposition has an intrinsic beneficial component of rapid solidification which results in a fine-scale homogeneous microstructure devoid of macroscopic segregation. Further, the process is capable of high throughput rates in excess of 20 kg/min. Key process parameters are superheat, atomizing gas pressure, the working distance and the substrate motion. Detailed descriptions of the Osprey process are given elsewhere [1-7].

Currently, the Osprey process is used to produce components of different shapes of a wide variety of materials. Sandvik Steel in Sweden is producing stainless steel tubing of 100-440mm diameter and up to 8m in length, with wall thicknesses up to 50mm. The US Navy has utilized the Osprey process to make tubes of IN625 [8]. Billets/disks in the size range 100-250mm dia. and up to 1m in height are being fabricated by Alcan (aluminum alloys and composites) [9], Sumitomo Heavy Industries in Japan, and the General Electric Corporation (Ni-base superalloys) [10]. A majority of the current production and development of flat/strip products is being conducted by Mannesman-Demag Huettentechnik in W. Germany who have spray deposited strip in the thickness range 5-10mm, up to 1m in width and several meters in length [1].

To date, Osprey processing conditions have been optimized on the basis of trial and error from which empirical relationships have been derived. To quantitatively predict and control preform geometry and microstructure during spray deposition, it is necessary to develop a knowledge base and quantify the effect of each process parameter on the integrity of the components produced. To this end, research at Drexel University over the past four years has focussed on a fundamental analysis of

the Osprey process and the development of an integral mathematical model. This research has been sponsored by the Office of Naval Research and the National Science Foundation [4,5,11].

OBJECTIVE AND SCOPE OF THE RESEARCH PROGRAM

Successful utilization of the Osprey process mandates shape control with accompanying metallurgical integrity. This requires an understanding of the combined effects of (i) the rate of metal deposition, (ii) rate of heat extraction and (iii) substrate motion. Due to the microscopic size of the droplets and the time scale of events occuring during spray deposition, it is difficult to assess experimentally the contributions of the process variables in terms of the integrity of the resulting preform. Furthermore, the measurements must not interfere with the deposition process; this requires the utilization of sophisticated, non invasive experimental techniques which are currently unavailable. Therefore, the approach of choice has been to analyze the Osprey process by developing a mathematical model and to assess its predictions via experimental techniques. Well established theoretical tenets of fluid mechanics, heat transfer and phase transformations have been combined to formulate the process model which describes :

(a) the velocity and enthalpy profiles of droplets in flight,
(b) temperature distribution in the consolidated material during, and after, deposition, and
(c) the build up of preform shape/geometry.

Concurrent experimental work was conducted to arrive at input parameters for the model and to assess model predictions. Predictions of the model can be used to determine the microstructure and shape of the preforms for given set of processing conditions.

Results of the model for part (a) and the formulations for part (b) were previously reported [4,5] and a summary of the these results is provided in the next section. In the current phase of the program, the model for droplet-gas interactions was refined. Specifically, the recalescence behavior of individual droplets was modified and cast into a "micro" model to include non-equilibrium kinetics during droplet solidification in flight. Then, the enthalpy/fraction liquid in the individual droplets was averaged at various flight distances to obtain the variation of the

fraction liquid in the *spray* as a function of flight distance. This is an important parameter in spray deposition since the operative distance between the atomizer and the substrate must be selected based upon the fraction of liquid in the spray upon impact.

Boundary conditions for the deposit heat transfer model were determined. The heat transfer coefficient at the deposit-substrate interface was measured with a heat flux sensor embedded within the substrate.

Movement of the substrate was incorporated into the model for deposit heat transfer to simulate the conditions during the build up of complex shapes. This model predicts the three dimensional shape/geometry of the preform produced under rotational and/or reciprocating motion of the substrate. It can also account for a tilt angle between the substrate and the axis of the spray. Hence it is now possible to optimize both geometry and solidification of the preform by manipulating the parameters of substrate motion and the process variables which determine the condition of the spray at impact.

PREVIOUS WORK

In this section, we give a consise overview of completed research on this program. The Osprey process was analyzed in component stages which occur in sequence: (i) droplet-gas interactions in the metal spray, and (ii) droplet consolidation at the substrate, Fig. 2. Modeling and experimental work in these stages is then synthesized into an integral process model. Herein, the enthalpy and droplet mass distribution in the metal spray at impact (i.e. deposition condition) obtained from the first stage become inputs to the second stage of droplet consolidation. In this way, it is possible to simulate the thermal profiles in the metal spray, and the consolidated material, during spray deposition. Significant results are provided for those combinations of the major processs parameters typically in use in the Osprey process.

1. Droplet-Gas Interactions:

- The log-normal distribution of droplet sizes in the metal spray follows a bell-shaped curve with a mass-median diameter of ~80μm and standard deviation of 1.75 for Fe- and Ni-base alloys. The size distribution by *population* was found to be bi-modal, indicative of a disproportionately large fraction of fine droplets in the spray.
- From the model of droplets in flight, it is predicted that the velocity of droplets of Fe- and Ni-base alloys at impact is in the range 30-100m/s for droplet sizes from 20-150μm.
- From theoretical calculations, and the measurement of the extent of droplet solidification during flight, the degree of droplet undercooling f (= fraction of undercooling required for homogeneous nucleation) is found to decrease exponentially with increasing droplet volume.
- The spatial distribution of droplet mass (i.e. mass flux) in the spray is measured by a video camera to be nearly gaussian, and has its maxima at the spray axis. The dependence of deposition rate D on the radial distance from the spray axis, R, fits the following equation for a gaussian distribution:

$$D(R) = dL/dt = D_{max} \exp(-bR^2)$$

where D is expressed in mm/s, L is the thickness of the deposit at time t, D_{max} is the maximum deposition rate at the spray axis (= 5.25mm/s), and b is the radial distribution coefficient that governs the spread of the spray (= 0.0018mm^{-2}).

2. Droplet Consolidation at the Substrate:

- In the initial stages of deposition, the deposit solidification rate is greater than the heat influx, and therefore impinging droplets impact a solidified top surface of the growing deposit. This rapid cooling results in a high degree of interconnected porosity (~14%) in the first millimeter of the deposited material.
- With continued deposition, the rate of deposit solidification decreases and the temperature at the top surface of the deposit begins to rise. In this manner, a partially liquid layer forms on the surface of the deposit and increases in thickness with deposition time. The deposit comprises of two "layers" during its build up: (i) a bottom layer of solidified metal, and (ii) a partially liquid layer which contains

decreasing amounts of solid from bottom to top (fs=1.0-0.75). By the end of the spray deposition cycle (40s) less than 25% of the deposit thickness is fully solidified; the remaining material is in a mushy state containing a high fraction of solid.

- From the predicted thermal profiles across the deposit, and from temperature measurements within the sprayed deposits, it is concluded that the cooling rates during solidification of the bulk of the deposit are $<5^{o}C/s$.
- The deposits exhibit a fine scale, homogeneous microstructure. Measured values of grain/cell size in the deposit are approximately equal to, or less than, the mean droplet diameter and are *smaller* than values of the same computed from the cooling rates (i.e. dendrite arm coarsening models). Hence, the relationship between the temperature profiles and microstructure in sprayed preforms is <u>not</u> understood. It is possible that the solidification in sprayed deposits involves a high density of nucleating sites and may be analogous to liquid phase sintering in a two phase slurry of the partially liquid layer. Hence the characteristics of the liquid layer govern the microstructure of the deposit (i.e. porosity, grain size, ...).

PROGRAM STATUS

The overall approach of the research program is depicted in Fig. 2. Various aspects of the program which were addressed during this year are described.

1. Thermal Profiles of Droplets in Flight:

Droplets in the metal spray are initially at a temperature $T_L+\Delta T_s$ where T_L is the liquidus temperature and ΔT_s is the melt superheat. The droplets lose heat to the atomizing gas and cool during flight until the nucleation temperature is reached; this is determined from the measured values of the largest solidified droplet vs flight distance [4-7]. Subsequent recalescence and solidification of the droplets are modeled on a microscopic scale by monitoring the motion of the solid-liquid interface across the droplet volume, Fig. 3. The volume fraction solid for the axisymmetric growth geometry shown is related to the interface position by the following expressions:

$$f_s = (1/2)\,(1+z)^3 - (3/16)\,(1+z)^4$$
$$z = z^0 + V_{s-l} \cdot \Delta t$$

where f_s is the fraction solid, 1+z is the distance solidified in the droplet normailzed by the droplet radius, and V_{s-l} is the solid-liquid interface velocity which is calculated by the analysis of Langer and Muller-Krumbhaar [4-7,12]. Solute partitioning has been coupled to the solidification kinetics such that the partition coefficient $k = f(V_{s-l})$ [12,13].

The droplet temperature profiles obtained from the model are diplayed in Fig. 4(a) for three droplet diameters of Fe-5 w/o Ti alloy. It is observed that with increasing droplet diameter, (i) a smaller fraction of the droplet solidifies during recalescence up to the arrest temperature, and (ii) solidification occurs over a wide range of flight distance. Calculated recalescence and solidification of an 80μm droplet of Fe-5 w/o Ti are shown in Fig. 4(b) on a temperature vs composition diagram. The equilibrium phase diagram is superimposed on the figure for comparison. Upon nucleation at 1145°C, the droplet recalesces without partitioning (no segregation) up to 1286°C and about a third of the droplet mass is predicted to solidify during this time period of ~0.27μs.

Further solidification involves non-equilibrium partitioning of the solute and the paths of the liquid and solid compositions are depicted in Fig. 4(b) along with the projected dendrite growth velocities and progress of droplet solidification. Recalescence continues for a total period of ~11μs with progressively decreasing values of solidification velocity and partition coefficient until $C_l \approx C_{eq}$ at 1429°C (arrest temperature, T_a). Subsequently, droplet solidification occurs via equilibrium partitioning and cooling until the liquid composition reaches the eutectic.

The scale of the microstructure in the droplets substantiates the high rates of solidification predicted by the model (i.e. df_s/dt or dendrite growth velocities given in Fig. 4(b)). The observed microstructures of the powders indicate a high degree of compositional homogeneity across the dendrite arms/grains. However, it was not possible to establish the degree of partitionless solidification or non-equilibrium partitioning in the powders by microprobe analysis on the SEM due to the fineness of scale (beam diameter on SEM≈2μm).

Due to the non-equilibrium nature of solidification, droplet temperature and extent of solidification can be combined and represented by an equivalent enthalpy, H_d:

$$H_d = \int C_P \, dT + \int \Delta H_f \, df_s$$

where C_P is the specific heat and ΔH_f is the latent heat of fusion. H_d is used to represent the temperature and degree of solidification of the droplets at four selected flight distances, Fig. 5. Increasing the melt superheat or decreasing the atomizing gas pressure (i.e. velocity and flow rate) will shift the curves upwards. Indications are that the effect of melt superheat is less significant than the effect of gas pressure since superheat is quickly dissipated during the initial phase of droplet flight when the relative velocity is a maximum and the atomizing gas is at a low temperature.

The condition of the droplets arriving at the deposition surface (at spray heights in the range 300-400 mm) can be summarized as follows:
(i) droplets less than a critical diameter d* are completely solidified; typically d* is predicted to be in the size range 80μm-90μm for the alloys described. This corresponds to a significantly large fraction of presolidified droplets due to the bi-modal population distribution.
(ii) droplets with diameters greater than d* impact the deposition surface in a "mushy" condition with varying fraction of liquid, Fig. 5. These droplets comprise a solidified dendritic skeleton, as observed on the glass slides [4-7].
(iii) only droplets greater than about 700μm (at a superheat of 100°C) arrive at the deposition surface in a completely liquid state. However, the fraction of droplets with diameters greater than 700μm is extremely small under normal atomization conditions.

2. *Spray Characteristics as a function of Flight Distance:*

The heat content of the spray, $\bar{H}_{spray}$, is obtained by computing the weighted average of the enthalpy of droplets at selected flight distances. It is convenient to represent the calculated values of $\bar{H}_{spray}$ as the sum of two parts:

$$\bar{H}_{spray} = H_{solidus} + \Phi H_{fr}$$

where:
$H_{solidus} = {}_{25}\int^{T_s} C_P \, dT$ is the enthalpy of the alloy at the solidus temperature,
$H_{fr} = \Delta H_f + {}_{T_s}\int^{T_l} C_P \, dT$ is the total amount of heat in the freezing range, and Φ is a dimensionless constant. $\Phi = 0$ if the spray is totally solid, and $\Phi = 1$ if the spray is completely liquid.

The parameter Φ is chosen to represent the spray enthalpy since we consider that it dictates the outcome of the spray deposition process. If $\Phi=0$ at the deposition surface, the end result of spray deposition is powder production. At the other extreme, $\Phi=1$ is equivalent to conventional casting and a mold will be necessary to contain the flow of the liquid. The predicted variation of Φ with flight distance is given in Figure 6(a) for three alloys. Considering the Fe-20 w/o Mn alloy at a flight distance of 400mm, a value of $\Phi = 0.42$ signifies that 58% of the total heat in the freezing range has been released on arrival at the substrate.

The values of Φ were used to calculate the percentage of liquid in the spray as a function of flight distance; these values are shown in Figure 6(b). It is observed that the %liquid in the spray decreases rapidly in the initial stages (up to 100mm) and then the decrease is retarded. This behavior is due primarily to a decrease in the relative velocity between the droplets and the gas, and an increase in the temperature of the gas with flight distance. The condition of the spray at the deposition surface is thus derived from Fig. 6. For example, the calculations predict that, when spray depositing Fe-5 w/o Ti, 76% of the heat in the freezing range is released during flight and the remaining 24% is carried into the deposit. The spray comprises ~14% of liquid by weight.

Predicted values of Φ and liquid fraction in the spray at the deposition surface are at the low end of the range 0-1. This suggests that only a small fraction of liquid (<25%) is required to consolidate the presolidified droplets during deposition. It is therefore possible that the mechanism of droplet consolidation in spray deposition resembles liquid phase sintering. In this case, the packing density of the solidified droplets on impact will dictate the amount of liquid required for full densification.

During the build up of a deposit, the effective flight distance decreases with time and results in a corresponding increase in the enthalpy carried into the deposit, as shown in Fig. 6. It is inferred from the figure that the change in the value of ϕ during deposit build up becomes significant at operative flight distances less than about 300mm. Therefore, in order to maintain uniformity in deposition conditions, it is necessary to continuously increase the distance between the emplaced substrate and the point of atomization in order to maintain a constant spray height at the deposition surface.

3. *Boundary Conditions for the Deposit Heat Transfer Model:*

3.1 Deposit-Substrate Heat Transfer:

Heat transfer across the deposit-substrate interface is quantified by a flux Q_s across the interface, or by a heat transfer coefficient h_s. The heat flux was measured by a sensor embedded within the substrate; it consists of a copper disk (9.5mm dia. x 7mm thick) and an arrangement of three thermocouples as shown in Fig. 7. One thermocouple (TC_1) is soldered to the bottom surface of the disk, a second (TC_2) is inserted at its top surface and a third thermocouple (TC_3) is positioned 1mm above the top surface. The sensor is placed in a recess at the top surface of a zirconia-alumina refractory substrate and aligned along the axis of the spray. Data from the thermocouples were recorded on a 12-bit data acquisition system.

Heat flux into the top surface of the copper disk is calculated by using the measured temperatures TC_1 and TC_2 and conducting an inverse heat transfer analysis across the thickness of the copper disk. A one dimensional heat balance is established as follows:

$$\rho C (\partial T/\partial t) = (1/L^2) (\partial/\partial\eta (K \partial T/\partial\eta))$$

where L is the thickness of the disk, $\eta=z/L$, z is distance measured from the bottom surface, T is the temperature at position z and t is time elapsed from the start of deposition. The boundary conditions are:

$$T(\eta=1,t) = TC_2 (t)$$
$$T(\eta=0,t) = TC_1 (t)$$

The equations are solved by a finite difference scheme at nodes along the thickness of the disk to obtain the temperature distribution across the thickness at any time t. The heat flux Q_s and the heat transfer coefficient h_s are obtained from the temperature gradient at the top surface (η=1):

$$Q_s = K^n (T^n - T^{n-1})/\Delta z$$
$$h_s = Q_s / (TC_3 - T^n)$$

where n is the node at the top surface and Δz is the distance between the nodes n and n-1. This analysis provides the variation of Q_s and h_s as a function of time during the deposition period.

Temperature profiles recorded by the three thermocouples in the heat flux sensor during spray deposition of Fe-5 w/o Ti alloy are shown in Fig. 8(a). The heat flux Q_s calculated as a function of time by the inverse heat transfer analysis is shown in Fig. 8(b). Q_s rises rapidly to a maximum of ~40×10^6 J/m^2/s within a duration of approximately 1s from the start of deposition. Subsequently, the value of Q_s decreases with time.; this decrease can be divided into two stages which are delineated by an appreciable change in slope of the curve at t≈2.5s. This results from a separation between the deposit and the substrate and can arise due to contractional stresses within the solidifying deposit. The formation of an "air gap" between the deposit and the substrate has been observed experimentally, however it has not been possible to determine the time at which this event occurs.

3.2 Deposit-Gas Heat Transfer:

An order of magnitude value for deposit-gas heat transfer coefficient (h_g) is obtained by using an empirical formulation for convective cooling of flat plates by impinging gas jets [12,14]. This formulation relates h_g to the velocity and thermal properties of the impinging gas by the following expression:

$$(Nu / Pr^{0.42}) = (W/R) ((1-1.1W/R) / (1+0.1(\lambda/W - 6)W/R)) F(Re)$$

The function F(Re) is defined as:

$$F(Re) = 2\, Re^{0.5} (1 + Re^{0.55}/200)^{0.5}$$

The deposit-gas heat transfer coefficient is estimated as 200 $W/m^2/K$ from the above equations.

4. Preform Geometry and Thermal Profiles:

When a substrate/collector is introduced into the spray of droplets, the droplets impinge, consolidate and solidify on the substrate to form a deposit/preform. The flux of incoming droplets results in an increase in deposit thickness (due to mass flux) and a change in the thermal profiles in the deposit (due to heat and mass flux) as a function of time, Fig. 9. These effects are quantified by selecting a location P(x,y) on the substrate surface and establishing a balance between heat and mass influx from the metal spray and the rates of external heat extraction. Similarly, the analysis is repeated for different locations P(x,y) on the substrate surface which are defined by a two dimensional mesh of grid points, Fig. 9. This approach to determine the geometry of the preform and its thermal history is displayed in Fig. 2 and is described.

The heat and mass influx during a time step is governed by the radial distance $R_{(x,y)}$ between the location (x,y) and the axis of the spray. If the substrate is stationary, the value of $R_{(x,y)}$ is constant over the complete deposition cycle. If the substrate is non-stationary, $R_{(x,y)}$ changes with time according to the motion imparted to the substrate. The governing equations relating $R_{(x,y)}$ and t pertain to combinations of:
(a) substrate motion in the horizontal x-y plane with velocities V_x and V_y such that:

$$R_{(x,y)}\,(t+\Delta t) = [\,(X(t) + V_x\,\Delta t)^2 + (Y(t) + V_y\,\Delta t)^2\,]^{0.5}$$

where (X,Y) is coordinate of the point P(x,y) with respect to the spray axis.
(b) substrate rotation on its axis normal to the substrate surface at a rotation speed ω, such that:

$R_0 = [\,x^2 + y^2\,]^{0.5}$ is the distance between P(x,y) and the center of the substrate,

$$R_{(x,y)}^2\,(t+\Delta t) = [X^\circ + R_0 \cos\,\omega(t+\Delta t)]^2 + [Y^\circ + [R_0/\cos(90-\theta)]\,\sin\,\omega(t+\Delta t)]^2$$

where (X°,Y°) is the coordinate of the center of the disk with respect to the spray axis and θ is the tilt angle between the spray axis and the substrate surface, in the x-z plane.

Assuming that the tilt angle has a negligible effect on the deposition profile (i.e the flight distance does not change by tilting the substrate), the deposition rate $\dot{D}_{(x,y)}$ is :

$$\dot{D}_{(x,y)} = dL/dt = \dot{D}_{max} \exp(-b\, R_{(x,y)}^2)$$

and the thickness deposited after 'n' number of time steps is given by:

$$L_{(x,y)} = \sum_{i=1}^{n} \Delta L_{(x,y)i} = \sum_{i=1}^{n} \dot{D}_{(x,y)}\, \Delta t$$

Geometry of the preform is defined by a bounding surface which connects all points (x,y,L) where L is the calculated thickness at the grid point (x,y) on the substrate surface.

A three-dimensional representation of the final deposit shape after 40s of spraying onto a horizontal stationary substrate is shown in Fig. 10. Similarly, the geometry of a preform produced on a disc substrate (120mm dia.) rotating about its center (0,0) with the axis of the spray aligned 30mm from its center is displayed in Fig. 11. The predicted build up at two locations on the substrate surface (at the center of the disc R=0 and at a radial distance of 30mm) is also illustrated in Fig. 11. It is observed that the locations R=0 and R=30mm have nearly the same final thickness by the end of the deposition period (40s); thickness profiles and deposition rates, however, are not the same. This implies that uniformity in thickness of the final product does not ensure identical deposition cycles at all locations.

It is also possible to incorporate simultaneous rotational and reciprocating motions, and a tilt angle between the substrate and the horizontal, into the model to predict the time dependence of deposition rate and thickness. In turn, the resulting preform geometry of complex shapes can be predicted.

During deposition onto moving substrates, the time dependence of $\dot{D}$ is obtained from the model of substrate motion, as shown in Fig. 11. Temperature profiles in a preform during its build up on a substrate which is rotating under the spray are given in Fig. 12; the predictions apply to the location P(-30,0) in Fig. 11 rotating at ω=30 rpm. It is observed that the temperature of the top surface of the deposit oscillates in a cyclic manner corresponding to each pass under the spray. Oscillations in temperature are undesirable, particularly if they occur over a temperature range over which the surface temperature decreases below the eutectic. Under these conditions, the surface will solidify completely in the interval between two successive passes under the spray. This results in poor bonding between the "layers" thus produced. This problem is accentuated in materials with a high thermal conductivity/diffusivity (e.g. aluminum alloys), implying that the operative speeds of substrate rotation and/or reciprocation must be maintained at relatively higher values during spray deposition of these alloys.

CONCLUSIONS

- Droplets of Fe-5 w/o Ti less than 85μm in dia. are predicted to undergo an initial phase of partitionless solidification during recalescence.

- By summation of the enthalpy of individual droplets at a flight distance of 400mm, it is found that the spray retains 42% of the enthalpy in the freezing range of the Fe-20 w/o Mn alloy and ~7% of the enthalpy in the freezing range of Ni-20 w/o Cr. The percentage of liquid in the spray at the deposition surface (spray height of 400mm) is predicted to vary from 5% for Ni-20 w/o Cr to ~25% for Fe-20 w/o Mn.

- The percentage of liquid in the spray is found to decrease rapidly with increasing flight distance during the initial stages but subsequently the decrease is retarded. At operative flight distances of 300-400mm between the point of atomization and the deposition surface, the metal spray comprises 10-30 v/o liquid upon impact and droplets less than the mean droplet diameter are completely solidified.

• Deposit/preform geometry can be predicted by combining the variation of deposition rate across the spray cone with a mathematical description of substrate motion.

• Values of heat flux across the deposit-substrate interface, measured by a heat flux sensor within the substrate, are in the order of 40×10^6 J/m^2/s during the initial stages of deposition. The heat flux decreases rapidly to half this value in a period of 3-5 seconds, possibly due to the formation of an "air-gap" between the substrate and the solidifying deposit. The corresponding heat transfer coefficient is ~500W/m^2/K. Heat transfer coefficient at the deposit-gas interface is estimated as 200 W/m^2/K.

• Rotation and/or reciprocation of the substrate is found to result in a cyclic variation in temperature at (and near) the top surface of the deposit. This results in solidification of the top surface if the time period of the deposition cycle is less than the cooling rate on the top surface.

• The mathematical models provide a base to describe the geometry and microstructure of spray deposits and to quantify the effects of various process parameters.

REFERENCES

1. Leatham, A.G., Reichelt, W. and Metelmann, "*Near Net Shape Manufacturing Processes*", eds. Lee, P. W. and Ferguson, B. L., ASM International p. 259 (1988)

2. Evans, R.W., Leatham, A.G. and Brooks, R.G., *Powder Meatllurgy*, **28**, 1, p.13 (1985)

3. Apelian, D., Gillen, G. and Leatham, A., *"Processing of Structural Metals by Rapid Solidification"*, eds. Froes, F.H. and Savage, S.J., Amer. Soc. for Metals International, p.107 (1987)

4. Apelian, D., Lawley, A., Gillen, G. and Mathur, P., "Spray Deposition: A Fundamental Study of Droplet Impingement, Spreading and Consolidation", ONR Technical Report 3, NR 650-025, Contract N 00014-84-K-0472, Office of Naval Research, Arlington, VA (1986)

5. Apelian, D., Lawley, A., Gillen, G. and Mathur, P., "Spray Deposition: A Fundamental Study of Droplet Impingement, Spreading and Consolidation", ONR Technical Report 3, NR 650-025, Contract N 00014-84-K-0472, Office of Naval Research, Arlington, VA (1987)

6. Mathur, P.C., Apelian, D. and Lawley, A., *Acta Metall.*, in press (1988)

7. D. Apelian, A. Lawley, P. Mathur and X. Luo, *Modern Developments in Powder Metallurgy*, eds.: P. U. Gummeson and D. A. Gustafson, Metal Powder Industries Federation, Princeton, NJ, **18-21**, In Press (1988)

8 Moran, A. and Palko, W. A., in "Progress in Powder Metallurgy", eds. Freeby, C.L. and Hjort, H., Metal Powder Industries Federation, Princeton, NJ, **43** (1987)

9 Alcan, Kingston, Canada - private communication

10. Bricknell, R.H., *Met. Trans.*, **17A**, 4, p.583 (1986)

11. Lawley, A. and Apelian, D., "A Fundamental Study of Thin Strip Casting of Plain Carbon Steel by Spray Deposition", NSF Report MSM-8519047, National Science Foundation, Washington D.C. (1988)

12. Mathur, P.C., "*Analysis of the Spray Deposition Process*", Ph.D. Thesis, Drexel University, Philadelphia (1988)

13. Aziz, M.J., *J. Appl. Phys.*, **53**, p.1158 (1982)

14. Martin, H., *Advances in Heat Transfer*, eds. Harnett, J. P. and Irvine, T. F., Academic Press, **13** (1977)

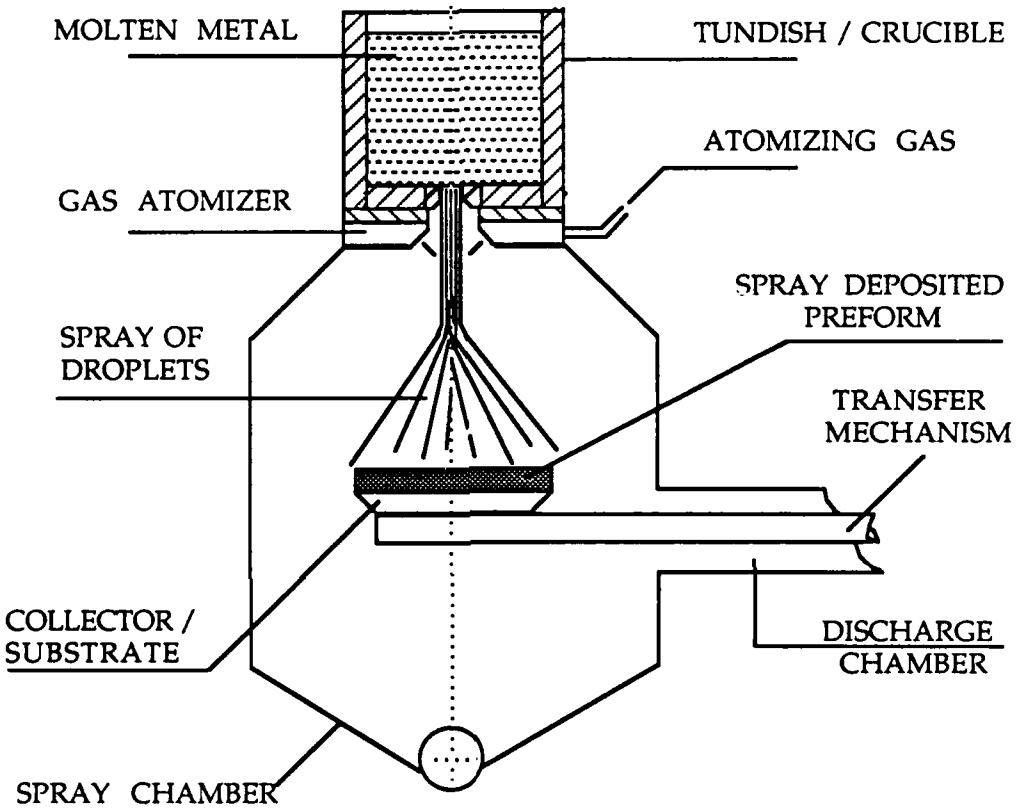

Fig. 1 Schematic of the Osprey™ Process

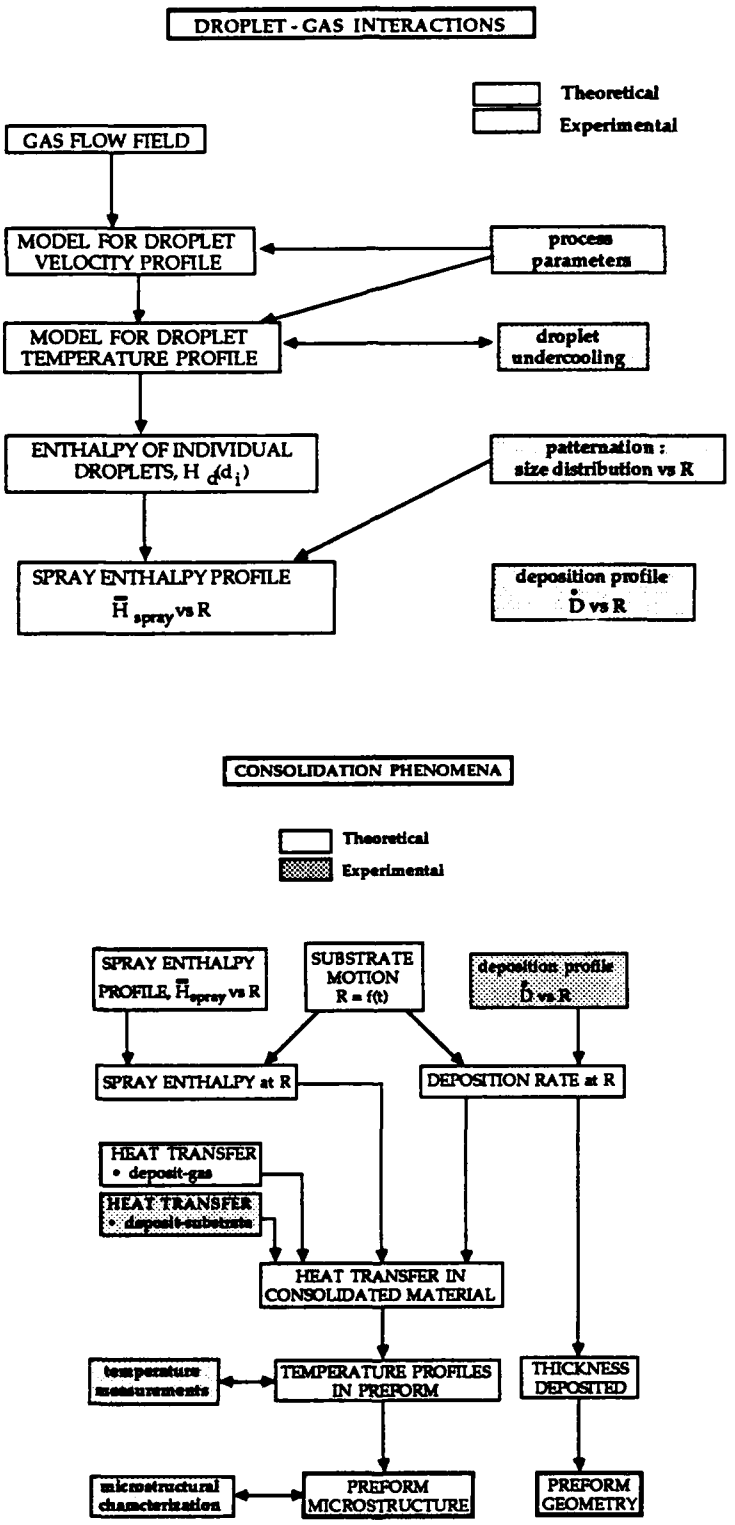

Fig. 2 Flow charts showing the approach adopted to analyze the Osprey spray deposition process

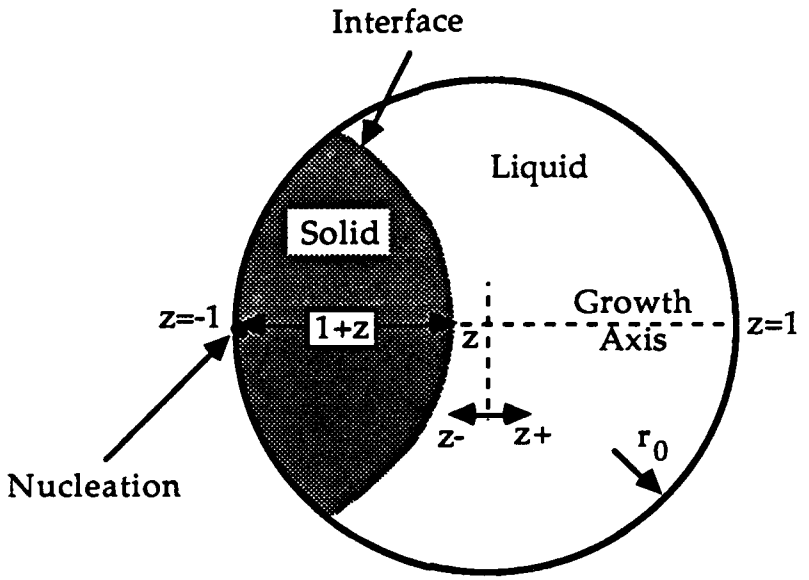

Fig. 3 Interface geometry used for analysis of undercooled solidification from a single nucleation event [12]

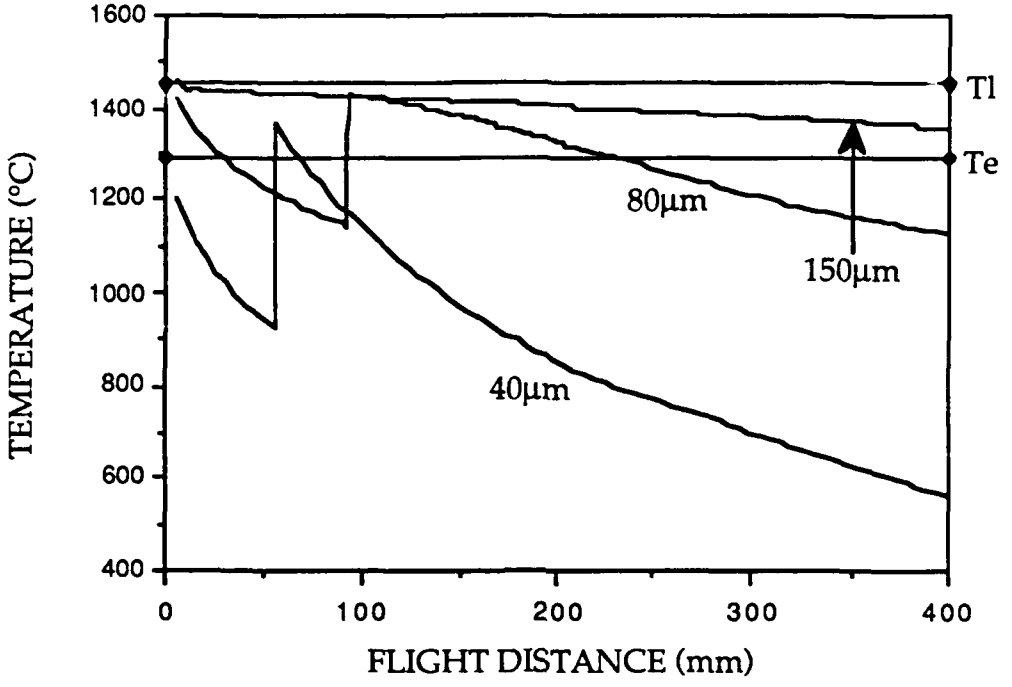

Fig. 4(a) Predicted temperature profiles of Fe-5 w/o Ti droplets during flight. Three droplet diameters are shown. Solidification is completed at the eutectic temperature, T_e

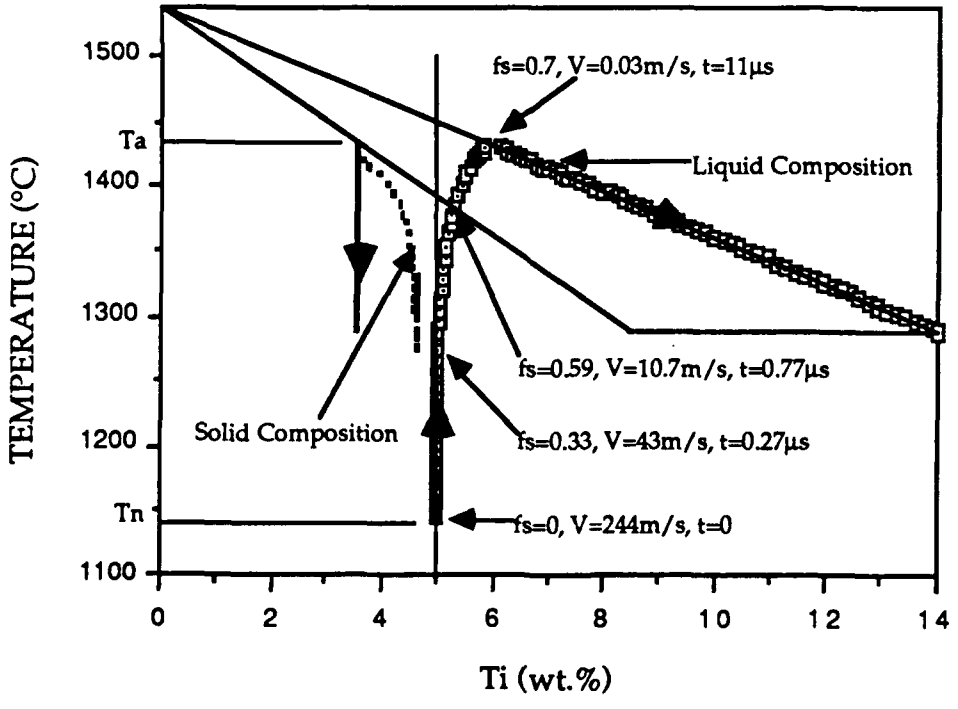

Fig. 4(b) Calculated recalescence and solidification of an 80μm droplet of Fe-5 w/o Ti showing nucleation at Tn, average composition of the solid and liquid during recalescence, the arrest temperature Ta and final solidification according to the Scheil equation

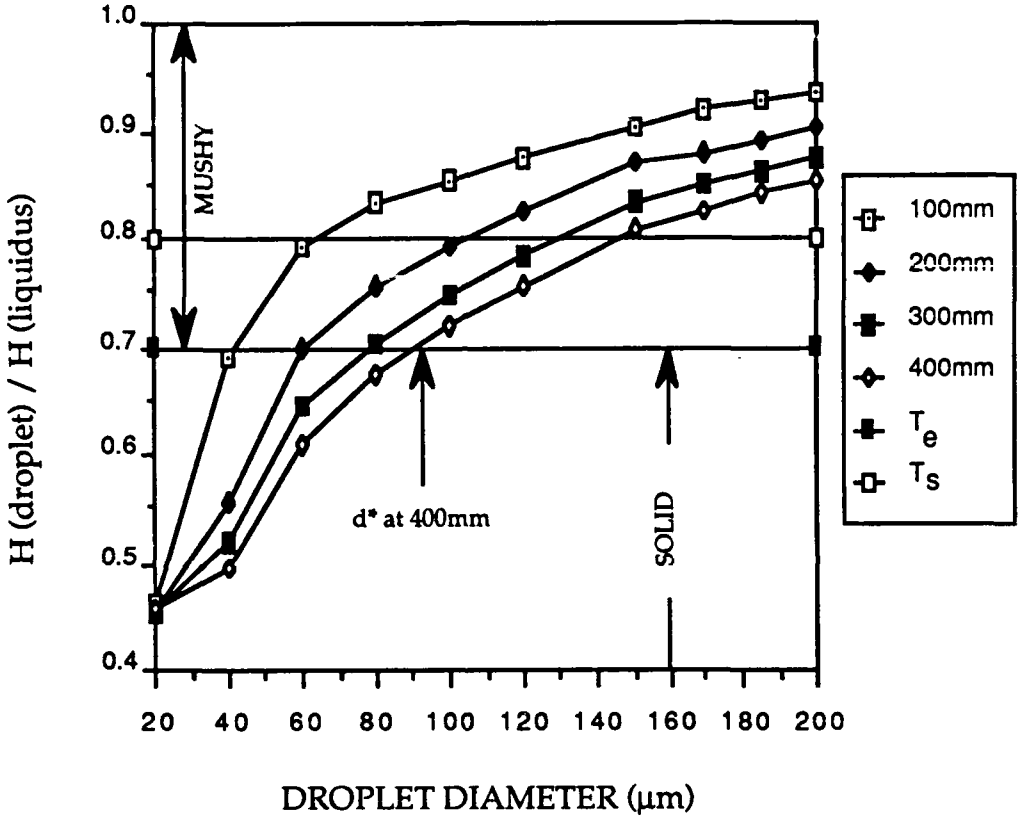

Fig. 5 Calculated variation of the normalized enthalpy as a function of droplet diameter at four flight distances; Fe-5 w/o Ti. Droplets with normalized enthaply less than 0.7 are fully solidified

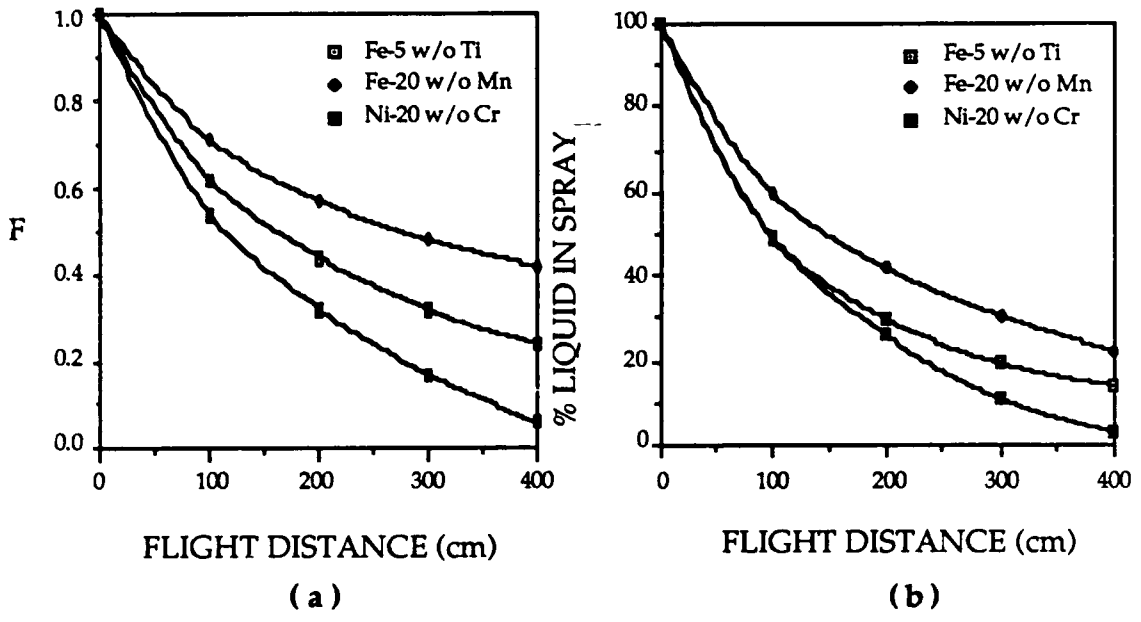

Fig. 6 The dependence of (a) calculated spray enthalpy (^{F}) and (b) percent liquid in the spray, with flight distance.

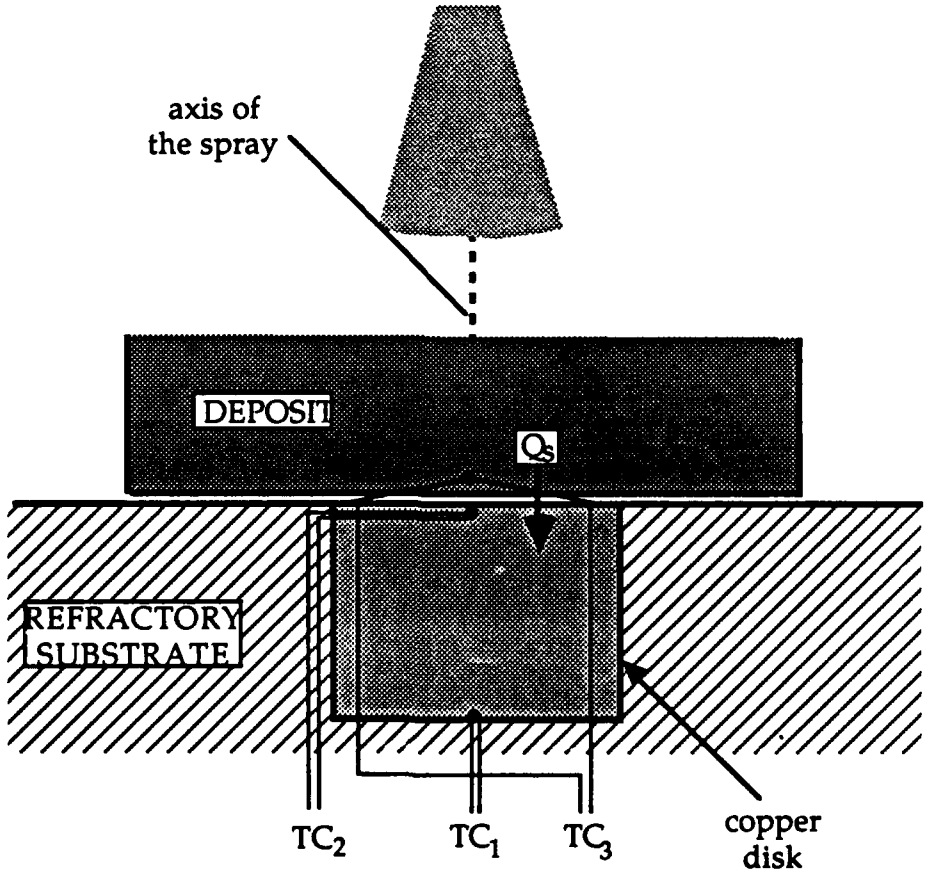

Fig. 7 Schematic arrangement of the heat flux sensor

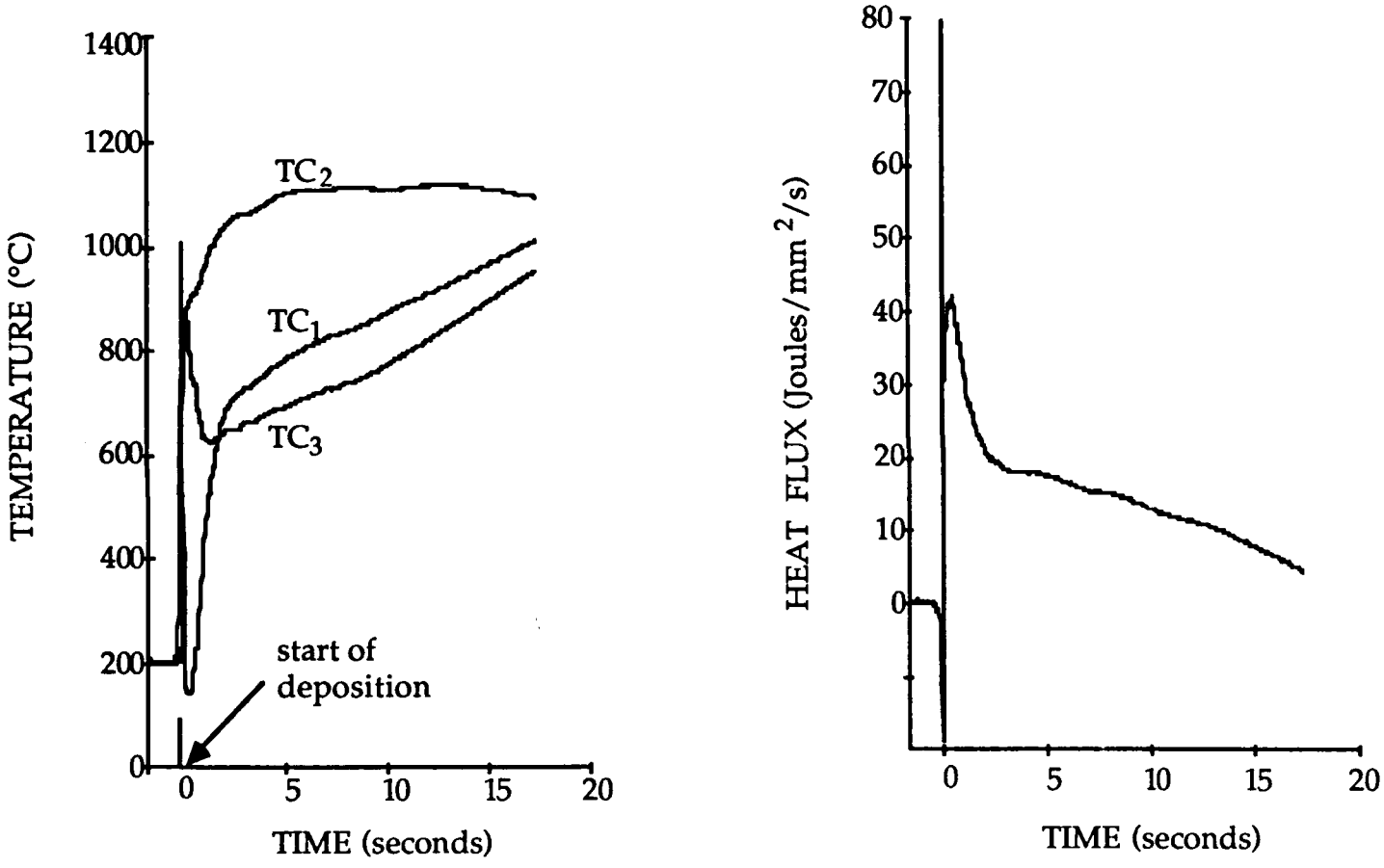

Fig. 8 (a) Measured temperature profiles in the heat flux sensor,
(b) calculated variation of heat flux across the
deposit-substrate interface

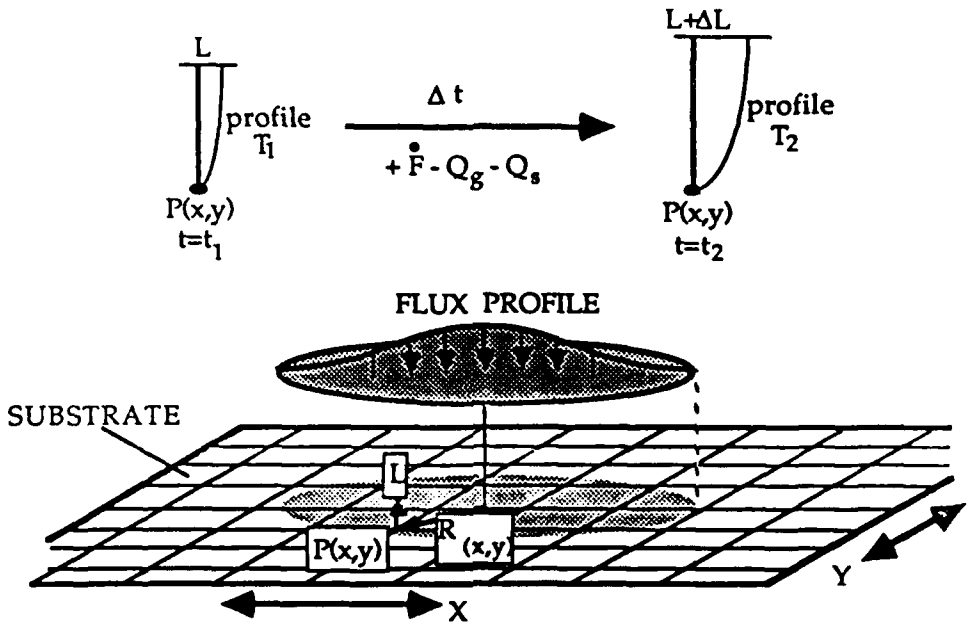

Fig. 9 Schematic showing the variation of thickness and temperature at a point P(x,y) on the substrate

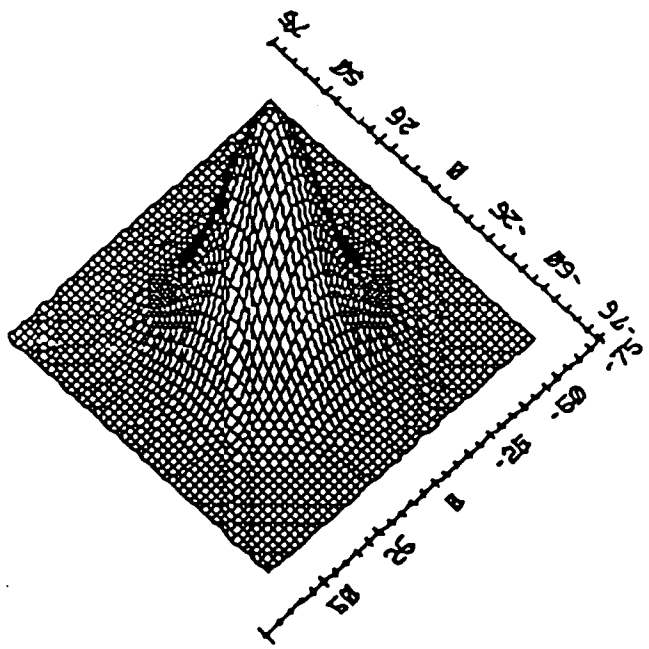

Maximum Height = 210mm

Fig. 10 Geometry of deposit produced on a horizontal stationary substrate

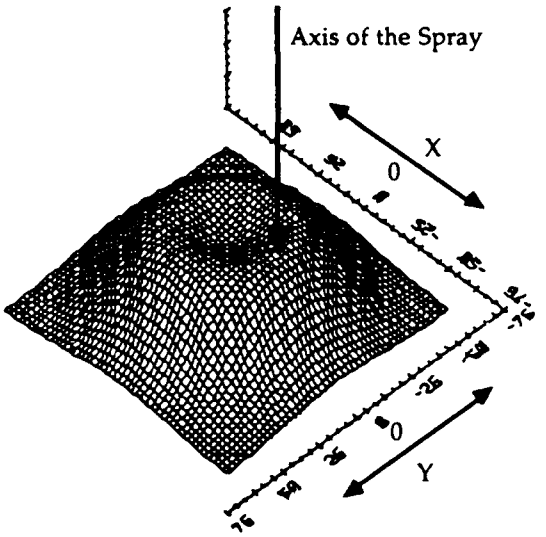

(a)

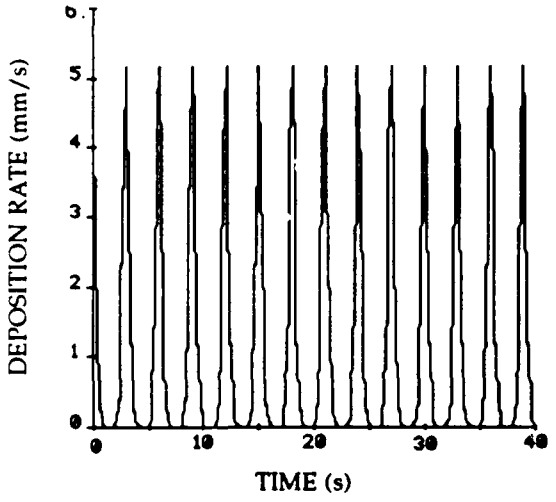

(b)

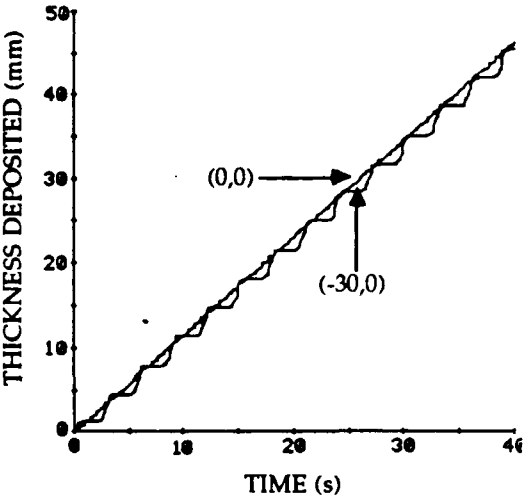

(c)

Fig. 11 (a) Geometry of preform produced by rotation about the origin (0,0) with the axis of the spray at (-30,0).
(b) Time dependent deposition rate at P(-30,0)
(c) Build up of the deposit at (-30,0) and (0,0) as a function of time

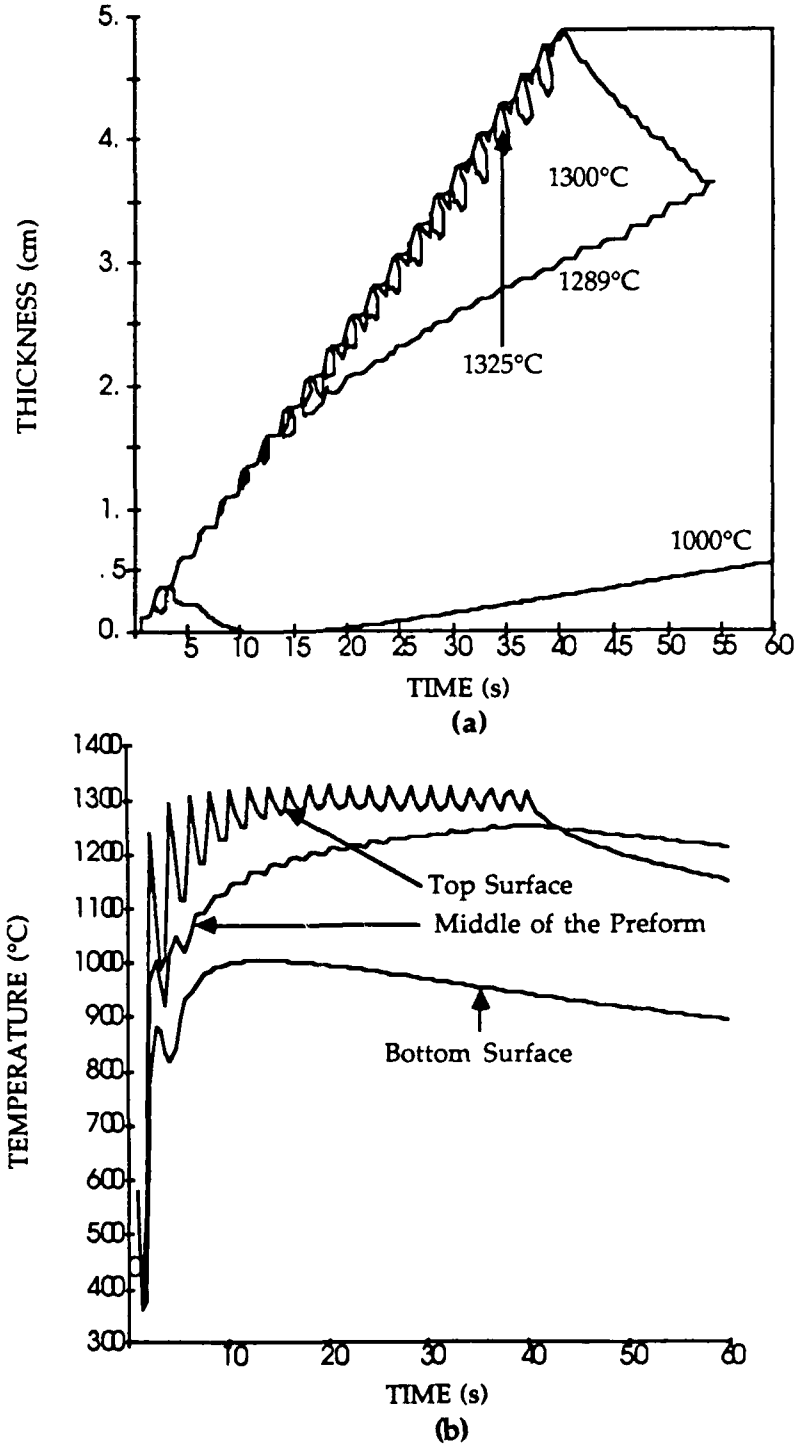

Fig. 12 (a) Thermal contours across Fe-5 /wo Ti deposit produced on a rotating substrate, Rotation speed = 30rpm, location (-30,0) in Figure 11, and (b) Temperature at the top, middle and bottom locations of the preform